34th Annual International Conference of the IEEE EMBS
San Diego, California USA, 28 August - 1 September, 2012

Computer-aided Diagnosis of Proliferative Diabetic Retinopathy

Faraz Oloumi[1] and Rangaraj M. Rangayyan[1*] and Anna L. Ells[2]

Abstract— **Monitoring the openness of the major temporal arcade (MTA) and how it changes over time could facilitate improved diagnosis and timely treatment of proliferative diabetic retinopathy (PDR). We present methods for user-guided modeling and measurement of the openness of the MTA based on a form of the generalized Hough transform for the detection of parabolas, and to compare it with a method of arcade angle measurement. The methods, implemented via a graphical user interface, were tested with retinal fundus images of 10 normal individuals and 15 patients with PDR. The results using the openness parameters of single- and dual-parabolic models as well as the arcade angle measurements indicate areas under the receiver operating characteristics of $A_z = 0.94$, 0.87, and 0.84, respectively. The proposed methods should facilitate improved quantitative analysis of the architecture of the MTA, as well as assist in detection, diagnosis, and improved treatment of PDR.**

I. Introduction

A. Changes in the Architecture of the Major Temporal Vessels

Various types of pathology, such as proliferative diabetic retinopathy (PDR), myopia, and retinopathy of prematurity (ROP) are known to affect the structure of the retinal vasculature [1]–[4]. The narrowing (or straightening) of the major temporal arcade (MTA) has been used as an indicator of compromised structural integrity of the macular region, which is responsible for visual acuity; such changes may result in loss of vision [1]–[5].

There has been an extensive amount of research conducted on computer-aided detection or diagnosis (CAD) of nonproliferative diabetic retinopathy (NPDR) [6]–[13]. Signs of NPDR include microaneurysms, cotton wool spots, hemorrhages, and changes in the tortuosity and width of retinal vessels [7], [8], [14]. However, it is only in the presence of PDR that the architecture of the MTA is known to be affected due to proliferation of fibrovascular tissue over the surface of the retina [1], [2]. Contraction of the retinal surface as well as the fibrovascular proliferation of the pathological tissue near the optic nerve head (ONH) cause traction of the arcades, tractional retinal detachment, macular dragging, and subsequently loss of vision [1], [2]. Even though such changes in the architecture of the MTA have been observed qualitatively, no quantitative analysis of the abnormal architecture of the MTA in the presence of PDR has been reported.

B. Quantitative Analysis of the Architecture of the MTA

In order to quantify the openness of the MTA, an angle of insertion of the MTA has been loosely defined as the angle between the superior and inferior temporal arcades (STA and ITA) as they diverge from the ONH towards the periphery of the retina [3], [4], [15].

Despite the clinical importance of abnormal changes in the architecture of the MTA, it has been quantified, in various manners, in only three studies: a study dealing with myopia [3] and two studies dealing with ROP [4], [15]. Even though the three studies have shown statistical significance of the changes in the MTA angles with respect to the stages of the diseases studied, they have used different definitions. Only the location of the vertex of the MTA angle has been consistently defined as the center of the ONH. The locations of the other two points used have been defined in different manners. Our implementation of the method of Wong et al. [4] has shown the differences between arcade angle measurements of normal cases as compared to cases with PDR to be statistically highly significant [16].

As shown in our previous studies [17], [18], the parabolic shape of the MTA, or the dual-parabolic nature of the STA and ITA, allow for effective single- and dual-parabolic modeling in an automated environment using a form of the generalized Hough transform (GHT). In such models, changes in the architecture of the MTA, STA, and ITA are expected to be reflected as changes in the openness parameters of the parabolic models.

The aim of the present study is CAD of PDR by quantitative measurement of the changes in the openness of the MTA due to PDR via single- and dual-parabolic modeling of the MTA, STA, and ITA, as well as measurement of the arcade angles via a graphical user interface (GUI) [16], [18].

II. Methods

A. Database of Fundus Images of the Retina

The proposed methods were tested with images from the STARE (STructured Analysis of the REtina) database [19]. The images of the STARE database have a size of 700×605 pixels and a field of view (FOV) of $35°$. The spatial resolution of the images is approximately 15 μm/pixel; however, the spatial resolution appears to vary from one image to another. Ten normal cases and 15 cases of PDR were obtained. The STARE database has 22 cases that are diagnosed with PDR; however, seven cases were not used because either the MTA was not in the FOV, or the major

This work was supported by the Natural Sciences and Engineering Research Council of Canada. We thank Dr. A. Hoover for help with the STARE images.

[1]Department of Electrical and Computer Engineering, Schulich School of Engineering, University of Calgary, Calgary, AB, Canada, T2N 1N4. *ranga@ucalgary.ca.

[2]Division of Ophthalmology, Departmant of Surgery, Alberta Children's Hospital, Calgary, AB, Canada, T3B 6A8.

vessels were not distinguishable. The PDR cases are not part of the publicly available subset of images of the STARE database and were provided by Dr. A. Hoover (Clemson University) upon request.

B. Arcade Angle Measurement Procedure

Selecting an image via the GUI prompts the user to mark the center of the ONH, after which a circle of radius $r = 120$ pixels is automatically drawn on the image. The user is then prompted to mark the point of intersection of the circle with the superior venule; the same is repeated for the inferior venule. The arcade angle is measured as the angle between the three marked points with the center of the ONH being the vertex, using $\arctan[(m_1 - m_2)/(1 + m_1 m_2)]$, where m_1 and m_2 are the slopes of the two lines and $m_2 > m_1$.

C. Overview of the Image Processing Methods

There are three main steps involved in the detection and modeling of the MTA, STA, and ITA, as performed using the GUI; these steps are only presented in point form, as they have been described in detail in our previous publications [17], [20].

1) Detection of blood vessels using Gabor filters [20]:
   a) Normalizing each color component in the original image.
   b) Computing the luminance component.
   c) Thresholding the luminance component to obtain the effective area.
   d) Extending the luminance component beyond the effective area to avoid the detection of its edges.
   e) Obtaining the Gabor magnitude response using 45 Gabor filters over the range of $[-90°, 90°]$.
2) Binarization of the detected vessels [17], [18]:
   a) Separating the Gabor magnitude response image into its superior and inferior parts to represent the STA and the ITA, respectively.
   b) Binarizing the Gabor magnitude response images of the MTA, the ITA, and the STA.
   c) Applying the morphological process of area open to filter the binary images.
3) Detection of parabolas and semiparabolas using the GHT [17], [18]:
   a) Skeletonizing the binary images.
   b) Reflecting each skeleton image from left to right if the MTA opens to the left (i.e., the image is of the right eye).
   c) Cropping each skeleton image horizontally.
   d) Applying the GHT to the preprocessed skeleton images of the MTA, the STA, and the ITA.
   e) Obtaining the parameters of the best-fitting parabolas from the resulting Hough space.

D. Detection of Blood Vessels and Modeling of the MTA

In order to detect the blood vessels, the user has the option of manually specifying the Gabor filter parameters [thickness (τ), elongation (l), and number of filters (K)]. As mentioned in Section II-A, the spatial resolution of the images of the STARE database may vary; hence, a large value for the thickness ($16 \leq \tau \leq 26$), with $l = 2$ is used to emphasize the presence of the MTA; the number of filters is kept constant at $K = 45$ (see references [17] and [20] for more details on Gabor filters).

The Gabor magnitude response image can be thresholded using a sliding threshold. In order to remove unwanted small vessel segments that may remain even after the thresholding step, the user can specify the maximum number of connected pixels to be removed (via the morphological operation of area open [21]) in the editable text field provided via the GUI.

The modeling procedure requires a binary image in order to perform the GHT procedure. The user has to first indicate if the current image is an image of the right eye or the left eye and is then prompted to mark the approximate location of the ONH in a separate window by clicking on the image. By default, the GUI leads to single-parabolic modeling; however, the user has the option of performing dual-parabolic modeling. The Gabor magnitude-updated version of the GHT with vertex restriction is used in the GUI (see reference [17] for more information). The range of the parameter a, used in the parabolic modeling procedure, was set to $20 \geq a \geq 420$ for the images of the STARE database.

To assess the diagnostic accuracy of the results of single- and dual-parabolic modeling, as well as the arcade angle measurements, receiver operating characteristic (ROC) [22] analysis was performed using the ROCKIT [23] software.

III. Results

Figure 1 shows the main window of the GUI and the "Open File" dialog box that allows for opening commonlly used types of image files. The three steps invovled in detection and modeling of the MTA, as explained in Section II-C, are implemented as separate modules in the GUI. The angle measurement procedure is also designed as a module.

For all of the images, $l = 2$ and $K = 45$ were used to detect the MTA. The range of values of τ used is $[16, 26]$, which was needed due to the large variability of vessel thickness in the STARE images. For each image, a different threshold was selected using the sliding threshold, provided by the GUI, to obtain a binary image containing only the MTA. Varying numbers of connected pixels were removed for each image to ensure that no vessel other than the MTA would influence the modeling procedure. On the average, it took about one minute to obtain the parabolic models (single and dual) for an image via the GUI using a Lenovo Thinkpad T510, equipped with an Intel Core i7 (Hyper-threaded-dual-core) 2.67-GHz processor, 4 MB of level 2 cache, 8 GB of DDR3 RAM, running 64-bit Windows 7 Professional, and using a 64-bit Matlab software.

For the arcade angle measurements, the method of Wong et al. [4], using a circle of radius 120 pixels, was used on all images. On the average, it took about a 30 seconds to obtain the arcade angle measure for a single image using the same system as explained above.

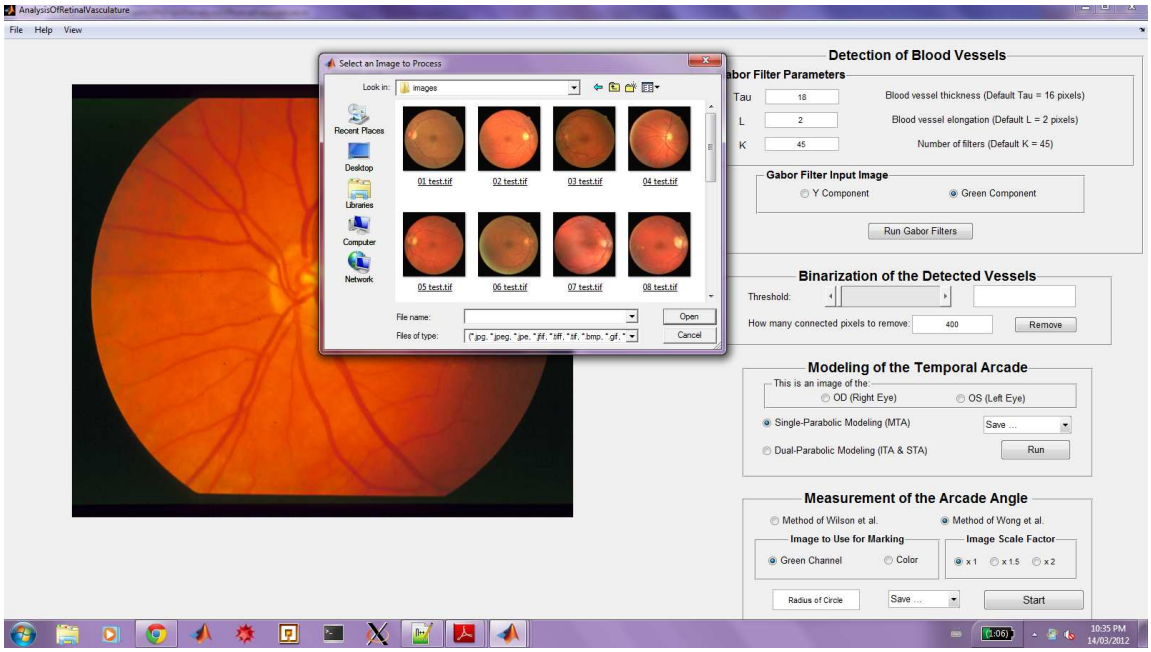

Fig. 1. The main GUI window showing a selected retinal image (im0080) form the STARE database and the "Open File" dialog box.

Figure 2 illustrates the results of dual-parabolic modeling and arcade angle measurement for a normal case as well as a PDR case. There are large differences between the values of the openness parameters of the ITA models obtained for the normal case as compared to the PDR case; the same is also true for the difference between the arcade angle measure (values given in the caption of Figure 2).

Table I provides the mean, standard deviation (STD), and area under the ROC curve (A_z) for the results of single- and dual-parabolic modeling, as well as the arcade angle measurements of the normal and PDR cases. The differences between the absolute value of the openness parameters of the MTA ($|a_{\mathrm{MTA}}|$) and the ITA ($|a_{\mathrm{ITA}}|$) models for the normal cases as compared to the PDR cases were found to be statistically highly signif cant (p-value< 0.01). The same is true for the differences between the arcade angle measures for the normal cases as compared to the PDR cases. The low mean obtained for the absolute value of the openness parameter of the STA models ($|a_{\mathrm{STA}}|$) for the normal cases can be due to the asymmetric nature of the STA and ITA in several of the STARE images used, where the STA has a narrower opening as compared to the ITA. The A_z values indicate high diagnostic accuracy for the detection of PDR cases using $|a_{\mathrm{MTA}}|$, $|a_{\mathrm{ITA}}|$, and the arcade angle measures.

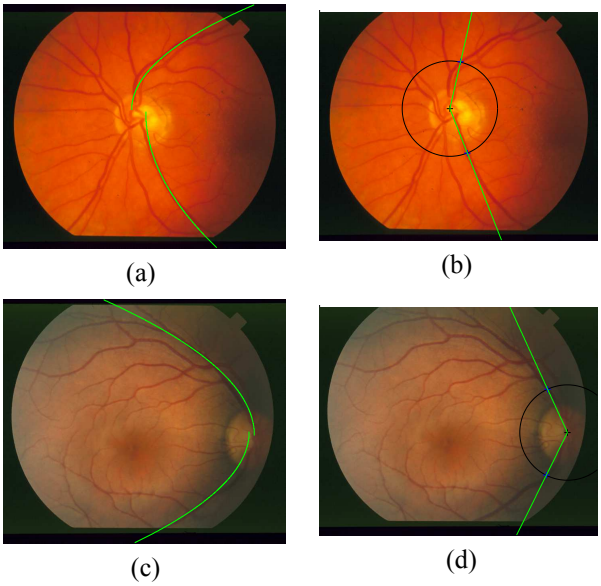

Fig. 2. (a) Dual-parabolic model ($a_{\mathrm{STA}} = 56$, $a_{\mathrm{ITA}} = 162$) and (b) arcade angle measure $= 153.2^{\circ}$ for image im0080 of the STARE database, which is a normal case. (c) Dual-parabolic model ($a_{\mathrm{STA}} = 76$, $a_{\mathrm{ITA}} = 67$) and (d) arcade angle measure $= 128.3^{\circ}$ obtained for image im0240 of the STARE database, which is a PDR case. It is clear that the ITA model provides better separation between the normal and PDR case as compared to the STA model. The arcade angle for the normal case is signif cantly larger than the arcade angle for the PDR case.

IV. Discussion and Conclusion

By combining time series of fundus images into short video clips, Ells and MacKeen [24] illustrated that the changes that occur in the MTA in the presence of progressive ROP are dynamic as they alter the posterior architecture of the MTA. Based on these observations, we believe that arcade angle measures may not accurately ref ect such changes that occur over the entire structure of the MTA, as they only def ne the openness of the MTA based on three points and are similar to f tting a triangle to the MTA.

Even though the $|a_{\mathrm{MTA}}|$ parameters of the normal and PDR cases have provided a larger A_z value than the $|a_{\mathrm{ITA}}|$

TABLE I

VALUES OF THE MEAN ± STD, AREA UNDER THE ROC CURVE (A_z), AND STANDARD ERROR (SE) FOR THE $|a|$ PARAMETERS OF THE SINGLE- AND DUAL-PARABOLIC MODELS, AS WELL AS THE ARCADE ANGLE MEASUREMENTS OBTAINED FOR NORMAL AND PDR CASES.

Parameter	Normal, ($n = 10$) Mean ± STD	PDR, ($n = 15$) Mean ± STD	A_z (SE)
Arcade Angle	151.41 ± 9.31	137.33 ± 10.67	0.84 (0.08)
$\lvert a_{\mathrm{MTA}} \rvert$	165.2 ± 60.41	85.07 ± 21.53	0.94 (0.07)
$\lvert a_{\mathrm{STA}} \rvert$	85.10 ± 27.89	76.4 ± 36.75	0.62 (0.11)
$\lvert a_{\mathrm{ITA}} \rvert$	186.8 ± 96.11	89.53 ± 58.86	0.87 (0.07)

parameters of the same cases, the results of single-parabolic modeling may be biased, because in cases of asymmetric arcades, the single-parabolic modeling procedure captures the more dominant parabola and may not incorporate both the STA and ITA. The dual-parabolic modeling procedure is more suitable for parameterization of the openness of the architecture of the MTA in fundus images of the retina.

Although the results are encouraging, a larger number of cases of PDR are needed for further analysis; however, the number of publicly available databases of retinal images that provide diagnostic information is limited. This is the first study to use quantification of the changes in the architecture of the MTA to perform diagnostic discrimination between normal cases and cases of PDR. Further work is in progress to evaluate the proposed methods with larger databases of cases of PDR as well as ROP, and to assess the significance of the differences between the A_z values related to the various parameters. The proposed methods could assist in quantitative analysis of the openness of the architecture of the MTA, and lead to improved diagnosis and clinical management of PDR.

REFERENCES

[1] Meier P and Wiedemann P, "Vitrectomy for traction macular detachment in diabetic retinopathy," *Graefe's Archive for Clinical and Experimental Ophthalmology*, vol. 235, pp. 569–574, 1997.

[2] Danis RP and Davis MD, "Proliferative diabetic retinopathy," in *Diabetic Retinopathy*, Duh EJ, Ed., Contemporary Diabetes, pp. 29–65. Humana Press, Totowa, NJ, 2008.

[3] Fledelius HC and Goldschmidt E, "Optic disc appearance and retinal temporal vessel arcade geometry in high myopia, as based on follow-up data over 38 years.," *Acta Ophthalmologica*, vol. 88, no. 5, pp. 514–520, 2010.

[4] Wong K, Ng J, Ells AL, Fielder AR, and Wilson CM, "The temporal and nasal retinal arteriolar and venular angles in preterm infants," *British Journal of Ophthalmology*, vol. 95, no. 12, pp. 1723–1727, 2011.

[5] Jelinek HF and Cree MJ, "Introduction," in *Automated Image Detection of Retinal Pathology*, Jelinek HF and Cree MJ, Eds., pp. 1–26. CRC Press, Boca Raton, FL, 2010.

[6] Abràmoff MD and Niemeijer M, "Detecting retinal pathology automatically with special emphasis on diabetic retinopathy," in *Automated Image Detection of Retinal Pathology*, Jelinek HF and Cree MJ, Eds., pp. 67–78. CRC Press, Boca Raton, 2010.

[7] Acharya R, Tan W, Yun WL, Ng EYK, Min LC, Chee C, Gupta M, Nayak J, and Suri JS, "The human eye," in *Image Modeling of the Human Eye*, Acharya R, Ng EYK, and Suri JS, Eds., pp. 1–35. Artech House, Norwood, MA, 2008.

[8] Patton N, Aslam TM, MacGillivray T, Deary IJ, Dhillon B, Eikelboom RH, Yogesan K, and Constable IJ, "Retinal image analysis: Concepts, applications and potential," *Progress in Retinal and Eye Research*, vol. 25, no. 1, pp. 99–127, 2006.

[9] Grisan E and Ruggeri A, "A divide et impera strategy for automatic classif cation of retinal vessels into arteries and veins," in *Engineering in Medicine and Biology Society, 25th Annual International Conference of the IEEE*, September 2003, vol. 1, pp. 890–893.

[10] Grisan E and Ruggeri A, "Segmentation of candidate dark lesions in fundus images based on local thresholding and pixel density," in *Engineering in Medicine and Biology Society, 29th Annual International Conference of the IEEE*, Aug 2007, pp. 6735 –6738.

[11] Niemeijer M, Abràmoff MD, and van Ginneken B, "Segmentation of the optic disk, macula and vascular arch in fundus photographs," *IEEE Transactions on Medical Imaging*, vol. 26, no. 1, pp. 116–127, 2007.

[12] Niemeijer M, Abràmoff MD, and van Ginneken B, "Information fusion for diabetic retinopathy CAD in digital color fundus photographs," *IEEE Transactions on Medical Imaging*, vol. 28, no. 5, pp. 775–785, 2009.

[13] Narasimha-Iyer H, Can A, Roysam B, Stewart CV, Tanenbaum HL, Majerovics A, and Singh H, "Robust detection and classif cation of longitudinal changes in color retinal fundus images for monitoring diabetic retinopathy," *IEEE Transactions on Biomedical Engineering*, vol. 53, no. 6, pp. 1084–1098, 2006.

[14] Worsley D and Simmons D, "Diabetic retinopathy and public health," in *Automated Image Detection of Retinal Pathology*, Jelinek HF and Cree MJ, Eds., pp. 27–66. CRC Press, Boca Raton, FL, 2010.

[15] Wilson C, Theodorou M, Cocker KD, and Fielder AR, "The temporal retinal vessel angle and infants born preterm," *British Journal of Ophthalmology*, vol. 90, pp. 702–704, 2006.

[16] Oloumi F, Rangayyan RM, and Ells AL, "A graphical user interface for measurement of temporal arcade angles in fundus images of the retina," in *Canadian Conference on Electrical and Computer Engineering (CCECE), IEEE Canada 25th Annual*, Montreal, Canada, 2012, p. 4, To be presented April 29-May 2.

[17] Oloumi F, Rangayyan RM, and Ells AL, "Parabolic modeling of the major temporal arcade in retinal fundus images," *IEEE Transactions on Instrumentation and Measurement (TIM)*, vol. -, pp. 13, 2012, In press.

[18] Oloumi F, Rangayyan RM, and Ells AL, "A graphical user interface for measurement of the openness of the retinal temporal arcade," in *Medical Measurements and Applications (MeMeA), IEEE International Symposium on*, Budapest, Hungary, May 2012, p. 4, To be presented May 18-19.

[19] "Structured Analysis of the Retina," http:// www. ces. clemson. edu /˜ahoover/ stare/, accessed Jan. 2012.

[20] Rangayyan RM, Ayres FJ, Oloumi Faraz, Oloumi Foad, and Eshghzadeh-Zanjani P, "Detection of blood vessels in the retina with multiscale Gabor f lters," *Journal of Electronic Imaging*, vol. 17, pp. 023018:1–7, April-June 2008.

[21] Acton ST, "A pyramidal algorithm for area morphology," in *Proceedings of IEEE International Conference on Image Processing*, Vancouver, BC, Canada, 2000, pp. 10–13.

[22] Metz CE, "Basic principles of ROC analysis," *Seminars in Nuclear Medicine*, vol. VIII, no. 4, pp. 283–298, 1978.

[23] "ROCKIT," Metz ROC Software. metz -roc .uchicago .edu /MetzROC /software.

[24] Ells AL and MacKeen LD, "Dynamic documentation of the evolution of retinopathy of prematurity in video format," *Journal of American Association for Pediatric Ophthalmology and Strabismus*, vol. 12, no. 4, pp. 349–351, 2008.